Lattice Boltzmann Flow Simulation in a Combined Nanochannel

Kazuhiko Suga[1,*], Susumu Takenaka[1], Takahiko Ito[1] and Masayuki Kaneda[1]

[1] *Department of Mechanical Engineering, Osaka Prefecture University, Sakai 599-8531, Japan*

Abstract. The widely used micro-flow wall-boundary conditions for lattice Boltzmann method (LBM) are evaluated in a force driven combined nanochannel flow. The flow field consists of a two-dimensional nanochannel (mother channel) of an infinite length having flat plates of a finite length inside. The flat plate is set above the bottom wall of the nanochannel with a narrow gap. The flow, thus, develops through this narrow gap (narrower channel) and the other side of the plate (wide gap). The Knudsen number based on the mother channel height is Kn=0.14 whereas the characteristic Knudsen number in the narrower channel is 1.1. To obtain the reference data, the molecular dynamics (MD) simulation is performed with a fully diffusive wall condition. The LBMs are based on the lattice BGK model and with the bounce-back/specular reflection (BSBC) and the diffuse scattering (DSBC) wall boundary conditions. The relaxation time is modified to include sensitivity to Kn. The DSBC shows generally satisfactory results in the test flow cases including fully developed force driven Poiseuille flows, where the BSBC performs worse at Kn>0.5 with a fixed bridge coefficient of b=0.7. This results in its overprediction of the flow rate in the narrower channel region since the characteristic Knudsen number there is 1.1. The MD simulation suggests that the flow develops gradually through the narrower channel region though all the LBM predictions show almost instant flow development. This fact suggests that the relaxation time model needs to have more sensitivity to the locally defined Kn. Further discussions of the BSBC with a different set of models suggest that the regularization process is required for predicting complex nanoscale flows.

---

*Corresponding author.
URL: http://www.me.osakafu-u.ac.jp/htlab/html-e/suga-profile-e1.html
Email: suga@me.osakafu-u.ac.jp (K. Suga), t.m1648@gmail.com (S. Takenaka), takaito@htlab.me.osakafu-u.ac.jp (T. Ito), mkaneda@me.osakafu-u.ac.jp (M. Kaneda)

1   Introduction

Due to the recent rapid development of micro flow devices applied in micro-total-analysis-systems (μ-TAS) and micro-electro-mechanical systems (MEMS), modeling and simulation methods for flows in such micro geometries have been of great interest in the society of computational physics [1]. Since the flow geometry in such systems is often in a sub-micron meter scale, those flows are usually distinguished by moderately high Knudsen numbers:

$$\text{Kn} = \frac{\lambda}{H} > 10^{-2},$$

where λ is the molecular mean free path of the fluid and H is the characteristic length of the flow domain. Accordingly, when one considers treating such flows, it is necessary to understand the flows at the molecular level. The continuum Navier-Stokes equations are, however, no longer applicable to such levels of moderately high Knudsen number flows and the flow physics in such flows is described by the Boltzmann equation (BE) of the gas kinetic theory [2,3]. Although several numerical schemes have been proposed for solving micro flows, amongst them, the lattice Boltzmann method (LBM) has been proven as an effective scheme because of its kinetic origin and numerical efficiency. Indeed, the LBMs have been well investigated in micro flows so far [4–13].

At a finite Kn, the statistical fluid dynamics indicates that the fluid in the vicinity of a solid wall should have a net motion relative to the wall. In the LBMs, there have been several schemes to treat this slippage at a wall boundary in micro flows. By the conventional bounce-back wall boundary condition, Nie et al. [4] simulated 2-D microchannel and cavity flows at $0.01 < \text{Kn} < 0.4$ introducing Knudsen number dependency into the relaxation parameter of the lattice Boltzmann equation. Shen et al. [9] validated this strategy comparing with the direct simulation Monte Carlo (DSMC) computations of microchannel flows. Succi [5] introduced a mix of bounce-back and specular reflections for the wall boundary condition. Toschi and Succi [10] tested a virtual wall collision concept into the bounce-back and diffuse scattering boundary conditions. The diffuse scattering boundary condition was firstly proposed by Ansumali and Karlin [6]. Zhang et al. [11] applied Maxwellian scattering kernel to the wall conditions with an accommodation coefficient. Verhaeghe et al. [13] proposed a diffuse bounce-back model for fully diffusive stationary walls. The present authors' group [12] also discussed a strategy to simulate such flow topics by the LBM where the diffuse scattering wall boundary condition and the effective relaxation time associated with the Knudsen number are applied. In our LBM, since at least third-order Hermite expansion is required to model the momentum equation at the Burnett level for isothermal and small Mach numbers, the higher order discrete velocity model: D2Q21, model was used. Moreover, to guarantee the nonequilibrium moments of the LBM satisfied in the Hermite space, a modified regularization procedure [14] of the nonequilibrium part of the distribution function was introduced. The results were

validated with the results of the DSMC in Couette and Poiseuille flows. Guo and Zheng [15] summarized these wall boundary treatments and showed that the bounce-back/specular-reflection, the diffuse scattering and the diffuse bounce-back models are all mathematically equivalent for prescribing the slip velocity at the wall.

As mentioned above, most of the schemes have been evaluated only in canonical flows such as gaseous flows through long microchannels, fully developed pressure-driven microchannel flows and Couette-Poiseuille flows. (There were some examples of application of the LBMs for a flow through a micro porous medium (e.g., [16]) though their accuracy is unknown due to the lack of reference data.) All these flow geometries are bounded only two simple flat walls though there is no doubt that these canonical flow cases provide essential flow physics and they are fundamental flows of a wide range of applications in microdevices. However, it is certainly necessary to evaluate the schemes in more complex flow fields which include other essential flow physics. In those canonical flows, one does not need to hesitate to choose the characteristic length H since they all have a single constant height of the flow passages. However, in practical complex flow applications, one has several options to define the characteristic length. Hence, there have been some questions arisen about the model performance on the Knudsen number dependency of the LBMs in complex flow geometries.

Therefore, the present study tries to evaluate the LBMs in a test flow case with a variable characteristic length. The considered flow geometry is still simple but consists of two channel regions: one is a nanochannel with a finite length (narrower channel) which is inserted in another larger infinite nanochannel (mother channel). The height ratio of the two channels is 0.125. The simulated representative Kn based on the height of the mother channel is Kn=0.14, at which the flow shows slippage at a solid wall. However, with such a height ratio, the characteristic Knudsen number in the narrower channel is 1.1. In order to provide the reference data, the molecular dynamics (MD) simulation using the Lennard-Jones potential [17] is also performed with "fully diffusive" walls. The presently evaluated LBMs are the LBMs based on the lattice BGK model with the bounce-back/specular-reflection boundary condition (BSBC) and the diffuse scattering boundary condition (DSBC) models.

2   Lattice Boltzmann method

A brief description of the lattice Boltzmann equation (LBE), which is the fundamental equation of the LBM [18, 19] and its steps of the application to high Knudsen number flows are given below.

The LBE can be obtained by discretizing the velocity space of the BE into a finite number of discrete velocities $\xi_\alpha\{\alpha=0,1,\cdots,Q-1\}$. Although many techniques to discretize the velocity space have been proposed, the present study employs so called D2Q9 and D2Q21 discrete velocity models as shown in Fig. 1. Table 1 lists the sound speed c_s, the discrete velocity ξ_α and the weight parameter ω_α in the models. Let $\mathbf{x}$ be

Table 1: Main parameters of the discrete velocity models for 2-D flows.

models	c_s^2	ξ_α	ω_α	
D2Q9	1/3	$(0,0)$	4/9	$(\alpha = 0)$
		$(\pm 1,0), (0,\pm 1)$	1/9	$(\alpha = 1\text{-}4)$
		$(\pm 1, \pm 1)$	1/36	$(\alpha = 5\text{-}8)$
D2Q21	2/3	$(0,0)$	91/324	$(\alpha = 0)$
		$(\pm 1,0), (0,\pm 1)$	1/12	$(\alpha = 1\text{-}4)$
		$(\pm 1, \pm 1)$	2/27	$(\alpha = 5\text{-}8)$
		$(\pm 2,0), (0,\pm 2)$	7/360	$(\alpha = 9\text{-}12)$
		$(\pm 2, \pm 2)$	1/432	$(\alpha = 13\text{-}16)$
		$(\pm 3,0), (0,\pm 3)$	1/1620	$(\alpha = 17\text{-}20)$

the Cartesian coordinates of the configuration space and ξ that of velocity space. The LBE describes evolutions of a single particle distribution function $f(\mathbf{x},\xi,t)$ defined such that $f(\mathbf{x},\xi,t)d\xi d\mathbf{x}$ represents the number of particles in the phase space element $d\xi d\mathbf{x}$ at time t, and can be written in the following BGK form [20]:

$$
\begin{aligned}
&f_\alpha(\mathbf{x} + \xi_\alpha \delta t, t + \delta t) \\
&= f_\alpha(\mathbf{x},t) - \frac{\delta t}{\tau + 0.5\delta t}\left(f_\alpha(\mathbf{x},t) - f_\alpha^{eq}(\mathbf{x},t)\right) + \frac{\tau \delta t}{\tau + 0.5\delta t}F_\alpha(\mathbf{x},t),
\end{aligned} \tag{2.1}
$$

where the equilibrium distribution function f_α^{eq} is written as

$$
f_\alpha^{eq}(\mathbf{x},t) = \omega_\alpha \rho \left\{ 1 + \frac{\xi_\alpha \cdot \mathbf{u}}{RT} + \frac{1}{2}\left[\frac{(\xi_\alpha \cdot \mathbf{u})^2}{(RT)^2} - \frac{\mathbf{u}^2}{RT}\right] \right\}, \tag{2.2a}
$$

$$
\begin{aligned}
f_\alpha^{eq}(\mathbf{x},t) = \omega_\alpha \rho \Big\{ &1 + \frac{\xi_\alpha \cdot \mathbf{u}}{RT} + \frac{1}{2}\left[\frac{(\xi_\alpha \cdot \mathbf{u})^2}{(RT)^2} - \frac{\mathbf{u}^2}{RT}\right] \\
&+ \frac{1}{6}\left[\frac{(\xi_\alpha \cdot \mathbf{u})^2}{(RT)^2} - 3\frac{\mathbf{u}^2}{RT}\right]\frac{\xi_\alpha \cdot \mathbf{u}}{RT} \Big\}.
\end{aligned} \tag{2.2b}
$$

Eq. (2.2a) retains up to the second-order term in the Hermite expansion and used in the D2Q9 velocity model whilst Eq. (2.2b) retains further to the third-order term and used
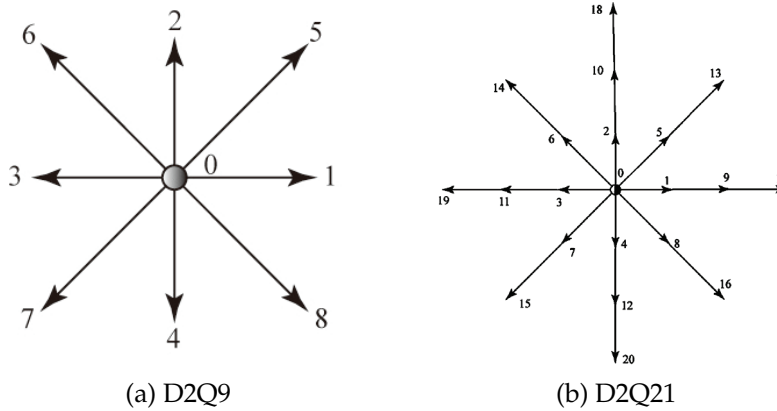

(a) D2Q9   (b) D2Q21

Figure 1: Discrete velocity models; (a) D2Q9 model, (b) D2Q21 model.

in the D2Q21 velocity model. The ideal gas constant is R, and ρ, $\mathbf{u}$ and T are respectively the fluid macro density, velocity and temperature. The sound speed $c_s = \sqrt{RT}$ is equal to $\sqrt{1/3}$ and $\sqrt{2/3}$ respectively in the D2Q9 and D2Q21 models. The contribution of the force term F_α is introduced respectively for the D2Q9 and D2Q21 models as

$$F_\alpha(\mathbf{x},t) = \omega_\alpha \rho \left\{ \left[\frac{\zeta_\alpha \cdot \mathbf{a}}{RT}\left(1 + \frac{\zeta_\alpha \cdot \mathbf{u}}{RT}\right) - \frac{\mathbf{a} \cdot \mathbf{u}}{RT}\right]\right\}, \tag{2.3a}$$

$$F_\alpha(\mathbf{x},t) = \omega_\alpha \rho \left\{ \left[\frac{\zeta_\alpha \cdot \mathbf{a}}{RT}\left(1 + \frac{\zeta_\alpha \cdot \mathbf{u}}{RT}\right) - \frac{\mathbf{a} \cdot \mathbf{u}}{RT}\right] \right. $$
$$\left. + \frac{1}{2\rho RT}\left[\sigma_{ij} + \rho \mathbf{u}^2\right] : \left[\frac{\zeta_\alpha \cdot \mathbf{a}}{RT}H^{(2)}\left(\frac{\zeta_\alpha}{RT}\right) - 2\frac{\mathbf{a}\zeta_\alpha}{RT}\right]\right\}, \tag{2.3b}$$

where $\sigma_{ij} = \sum_{\alpha=0}^{Q-1} f'_\alpha \zeta_{\alpha i}\zeta_{\alpha j}$, $\mathbf{a}$ is the acceleration and $H^{(n)}(x)$ is the n-th order Hermite polynomial of a variable x. The variables ρ, $\mathbf{u}$ and the pressure p are respectively obtained by applying the integral of microscopic velocity moment as

$$\rho = \sum_{\alpha=0}^{Q-1} f_\alpha, \qquad \rho \mathbf{u} = \sum_{\alpha=0}^{Q-1} f_\alpha \zeta_\alpha + \frac{\delta t}{2}\mathbf{a}, \qquad p = \rho c_s^2. \tag{2.4}$$

So far, the equations which govern the macroscopic variables of continuum flows are presented. Only when the non-equilibrium part of distribution is very small and the distribution function can be approximated by the equilibrium distribution function, the equations can describe the fluid phenomena. However, when the Kn becomes larger and the non-equilibrium part is no longer ignorable, the aforementioned LBE becomes invalid. According to our previous analysis [12], the difficulty is cleared by using the three procedures briefly described below (see [12] for more details).

2.1 Effective relaxation time

In continuum flow, the relaxation time τ can be defined in terms of viscosity η then flow is under control of the Reynolds number. In contrast, Kn is a fundamental dimensionless number in non-continuum flow. Therefore, for applying to high Kn flows, the relaxation time needs to be associated with Kn. Specifically, in microscale geometries, the relaxation time τ is influenced by the presence of walls and an effective relaxation time τ^*, which is a function of Kn has been applied instead of the relaxation time τ. With the bounce-back/specular-reflection boundary model, the following effective relaxation time:

$$\tau^* = \frac{\rho_{outlet} N_y \mathrm{Kn}_{outlet}}{\rho_{reference}\sqrt{\pi/6}} + \frac{1}{2}, \tag{2.5}$$

has been applied (e.g., [21]). Here, N_y is the characteristic lattice number. Note that this effective relaxation time is essentially constant in the whole computational domain.

The present authors' group used another effective relaxation time model [12]:

$$\tau^* = \tau \Psi(\mathrm{Kn}^*) = \sqrt{\frac{2}{\pi}}c_s H\mathrm{Kn}^* \Psi(\mathrm{Kn}^*), \tag{2.6}$$

where H is the characteristic length confined between walls in a microscale flow geometry and Kn^* is the local Knudsen number

$$\text{Kn}^* = \frac{\lambda}{H} = \frac{\eta}{\rho H}\sqrt{\frac{\pi}{2RT}}, \tag{2.7}$$

which varies depending on the local condition. The function Ψ can be expressed as

$$\Psi(\text{Kn}^*) = \frac{2}{\pi}\arctan(a\text{Kn}^{*-b}), \tag{2.8}$$

where the coefficient a and b are set $a=\sqrt{2}$ and $b=3/4$ (see [22]), based on the experiments. The functional behavior (Ψ decreases as Kn^* increases) indicates that some molecules will hit walls and their flight time (effective relaxation time τ^*) may be shorter than the mean free time (relaxation time τ) defined in an unbounded system.

2.2 Regularization procedure

Generally speaking, the distribution function f_α has an aliasing error because it cannot be entirely projected on to the Hermite space. Such an error is usually very small, but it can be no longer neglected, when the system is far from equilibrium because of high Knudsen number effects. To resolve this problem, the regularization procedure was previously introduced for improving numerical stability [14]. The procedure is implemented as the following. First, the distribution function f_α is divided as

$$f_\alpha = f_\alpha^{eq} + f_\alpha', \tag{2.9}$$

where f_α' is the non-equilibrium part of the distribution. Second, it is necessary to convert f_α' to a new distribution $\tilde{f}_\alpha'$ which lies within the subspace spanned by the first three Hermite polynomials. Using the Hermite polynomials, $\tilde{f}_\alpha'$ is expressed respectively for the D2Q9 and D2Q21 models as

$$\tilde{f}_\alpha' = \omega_\alpha \left[\frac{1}{2c_s^2} H^{(2)}\left(\frac{\xi_\alpha}{c_s}\right) \sum_{\alpha=o}^{Q-1} \tilde{f}_\alpha' \xi_{\alpha i}\xi_{\alpha j} \right], \tag{2.10a}$$

$$\tilde{f}_\alpha' = \omega_\alpha \left[\frac{1}{2c_s^2} H^{(2)}\left(\frac{\xi_\alpha}{c_s}\right) \sum_{\alpha=o}^{Q-1} \tilde{f}_\alpha' \xi_{\alpha i}\xi_{\alpha j} + \frac{B}{6c_s^2} H^{(3)}\left(\frac{\xi_\alpha}{c_s}\right) \sum_{\alpha=o}^{Q-1} \tilde{f}_\alpha' \xi_{\alpha i}\xi_{\alpha j}\xi_{\alpha k} \right], \tag{2.10b}$$

where, the coefficient B is given as

$$B = 1 - \Psi,$$

by substituting f_α in Eq. (2.1) to Eq. (2.9) after converting f_α' of Eq. (2.9) to Eq. (2.10a) or (2.10b), one can obtain the following form:

$$f_\alpha(\mathbf{x}+\xi_\alpha\delta t, t+\delta t) = f_\alpha^{eq}(\mathbf{x},t) + \frac{\tau - 0.5\delta t}{\tau + 0.5\delta t}\tilde{f}_\alpha' + \frac{\tau\delta t}{\tau + 0.5\delta t}F_\alpha(\mathbf{x},t). \tag{2.11}$$

2.3 Bounce-back/specular-reflection boundary condition (BSBC)

Succi [5] originally proposed the BSBC for slippage at a solid wall in a micro flow. Then, this simple scheme has been widely applied in flow simulations of in micro passages. In the BSBC scheme, it is assumed that some of the particles hitting a solid wall bounce back but the others reflect specularly. It is expressed as

$$f_\alpha(\mathbf{x}, t + \delta t) = b f_\beta(\mathbf{x}, t) + (1 - b) f_\gamma(\mathbf{x}, t), \tag{2.12}$$

where b is a bridge coefficient taking b=0.0-1.0 and vectors

$$\xi_\beta = -\xi_\alpha \quad \text{and} \quad \xi_\gamma = \xi_\alpha - 2(\xi_\alpha \cdot \mathbf{n})\mathbf{n},$$

are, respectively, the inverse and the specular symmetric velocity vectors of ξ_α with the unit wall normal vector $\mathbf{n}$.

2.4 Diffuse scattering boundary condition (DSBC)

The usual wall boundary conditions used in the LBM are based on perfect reflection, so the velocity and the temperature of a wall are not reflected into the distribution of the reflected particles. However, from a microscopic viewpoint, the wall boundary condition should include the physics on the wall because the fluid and the wall molecules are interacted with each other. Therefore, as Ansumali and Karlin [6] discussed the incident particles are modeled to be reflected with the information of the Maxwell distribution function at the wall boundary. The modeled form is written in the LBM frame as

$$f_\alpha(\mathbf{x}, t) = \frac{\sum_{\alpha'} |(\xi'_\alpha - \mathbf{u}_w) \cdot \mathbf{n}| f_{\alpha'}(\mathbf{x}, t)}{\sum_{\alpha'} |(\xi'_\alpha - \mathbf{u}_w) \cdot \mathbf{n}| f_{\alpha'}^{eq}(\mathbf{x}, t)} f_{\alpha,w}^{eq}(\mathbf{x}, t), \tag{2.13}$$

with

$$(\xi'_\alpha - \mathbf{u}_w) \cdot \mathbf{n} < 0, \qquad (\xi_\alpha - \mathbf{u}_w) \cdot \mathbf{n} > 0,$$

where $\mathbf{u}_w$ is the moving velocity of the wall, ξ'_α is the velocity of incident particles, $f_{\alpha,w}^{eq}$ is the wall equilibrium distribution function, and the subscripts w, α', α respectively denote the wall and the directions of the incident and reflected particles.

3 Molecular dynamics method

Molecular dynamics simulation consists of the numerical solution of classical equations of motion to calculate the motions of N molecules interacting via model potentials. One of the well-known model potential is the Lennard-Jones (6–12) potential ϕ, which is defined as

$$\phi(r) = 4\varepsilon \left[\left(\frac{\sigma}{r} \right)^{12} - \left(\frac{\sigma}{r} \right)^6 \right], \tag{3.1}$$

where r is the intermolecular distance, ε and σ are the well depth and the diameter of the molecules. This was used in the earliest study of the properties of argon. In the system which is modeled by the Lennard-Jones molecules only, the classical equation of motion can be rewritten as

$$\frac{d^2 r^*}{dt^{*2}} = -\frac{\varepsilon \tau^2}{m \sigma^2} \frac{\partial \phi^*}{\partial r^*}, \tag{3.2}$$

where

$$r^* = \frac{r}{\sigma}, \quad t^* = \frac{t}{\tau} = \frac{t}{\sqrt{m\sigma^2/\varepsilon}} \quad \text{and} \quad \phi^* = \frac{\phi}{\varepsilon},$$

are the nondimensional length, time and energy, respectively. However, to make a physical interpretation, it is sometimes expressed as finite values in terms of argon. In addition, the nondimensional number density $N^*=N\sigma^3$ and temperature $T^*=k_BT/\varepsilon$ are used in the Lennard-Jones fluid. (Here k_B is the Boltzmann constant.)

In actual calculations, to hold down the calculation effort of the interactions, the potential effects are truncated over cut off distance r_c, which is defined as $r_c=2.5\sigma$-5.5σ, In the present study, $r_c=3.0\sigma$ is employed.

3.1   The interactions between the fluid and wall molecules

When fluid flows in a finite space surrounded by walls, the flow is governed by the interaction between the fluid and the wall molecules. Thus, it is necessary to evaluate the flow phenomena in terms of the intermolecular potential energy between the fluid and the wall, which varies with the structures and the properties of the system.

In this study, the wall is simulated by an argon atom monolayer, which is schematically shown in Fig. 2. Wall molecules form regular triangles whose side length of $r_w=0.7$. Each of the wall molecules is tethered to fixed lattice site locations by harmonic springs with a large spring constant.

A fluid molecule is located near the wall molecules with the distance of r_0. Each of interactions between two molecules is the Lennard-Jones potential itself. However, the total wall-fluid interaction should include not only the nearest neighboring molecule but also surrounding ones. Therefore, the effects of the surrounding molecules are considered by the numbering molecules as follows: the nearest neighboring molecule is numbered $n=1$, and its surrounding six molecules are numbered $n=2$. Then the number of next twelve molecules around those numbered $n=2$ are defined as $n=3$. From this numbering rule, the potential energy between the fluid molecule and the wall molecules up to $n=k$ is written as the following
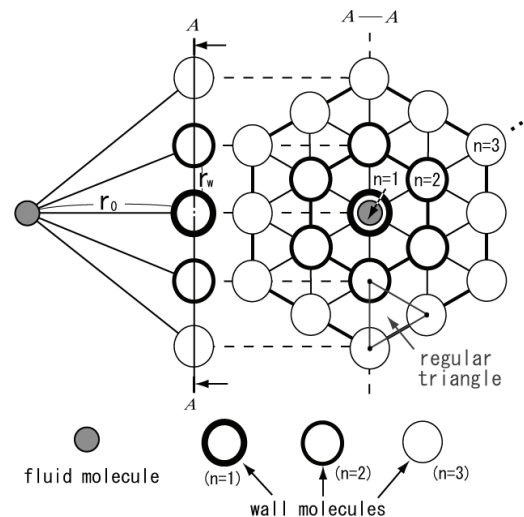

Figure 2: Schematic drawing of the wall structure. The left hand side is an edge view, and the right hand side is a schematic elevation of the wall.

form:

$$\sum_{n=1}^{k} \phi_n(r_0) = A \Bigg\{ 4\varepsilon \bigg[\Big(\frac{\sigma}{r}\Big)^{12} - \Big(\frac{\sigma}{r}\Big)^{6} \bigg] + 4\varepsilon \bigg[\Big(\frac{\sigma}{\sqrt{r_0^2 + r_w^2}}\Big)^{12} - \Big(\frac{\sigma}{\sqrt{r_0^2 + r_w^2}}\Big)^{6} \bigg] 6$$

$$+ \cdots + 4\varepsilon \bigg[\Big(\frac{\sigma}{\sqrt{r_0^2 + [(k-1)r_w]^2}}\Big)^{12} - \Big(\frac{\sigma}{\sqrt{r_0^2 + [(k-1)r_w]^2}}\Big)^{6} \bigg] 6(k-1) \Bigg\}, \quad (3.3)$$

where A is the parameter which determines the strength of the wall-fluid interaction. The present study sets $A=1$ after a series of validity tests. It was found that the potential energy almost converges by the stage of $\Sigma\phi$ up to $k=5$. And the well depth of the actual potential $\Sigma\phi$ up to $k=5$ is about 7.5 times as large as that of the Lennard-Jones potential. The features of the flows differ by the variation of this well depth. It is thus important to set appropriate parameters such as A, k and r_w according to the flow conditions. Note that the present set of parameters are tuned particularly for flows at Kn $\simeq 0.1$ referring to the DSMC data in the literature.

3.2   Definition of the molecular mean free path

The molecular mean free path length λ depends on the property of the system and the kind of the particles. The estimation method for λ used in the present study is as follows.

First, a one-dimensional model of inter-molecular collision is considered. Using the principle of equipartition of energy, the kinetic energy of a molecule with the velocity v is equal to the mean energy

$$\frac{1}{2}mv^2 = \frac{3}{2}k_B T, \quad (3.4)$$

when the molecules collide, the kinetic energy of the molecule is replaced with an equal volume of the potential energy. Thus, the following formula is obtained by the conservation law of energy:

$$\phi_{LJ}(r_m) = \frac{1}{2}mv^2 = \frac{3}{2}k_B T, \quad (3.5)$$

where r_m is the closest distance for the intermolecular collision. A repulsion force $F(r_m)$ is defined as a threshold value, which is determined whether the collision is present

$$F(r_m) = -\Big(\frac{d\phi_{LJ}}{dr}\Big)_{r_m}. \quad (3.6)$$

If the force acting on the molecule exceeds the threshold value, a collision occurs. To calculate the mean free path length, practically, the motion and the force of sample molecules are traced. The time interval between a collision point (the point when the force steps over the threshold value) and next collision point is a mean free time. Obviously, the migration distance in the mean free time is the mean free path length. Finally, the mean free path is obtained by taking the reasonable statistics of the migration distance.

4   Results and discussions

Before discussing the combined nanochannel flow, simulation results of canonical Poiseuille flows are discussed for the confirmation of the computer code and the model performance.

Then, the combined nanochannel flow is discussed. In the MD simulation, Kn is a resultant value of the computation and Kn=0.14 (this Kn is based on the single representative channel height) has been obtained at the present simulation. In order to compare the results, such a Kn is used as a computational condition of the LBM simulation.

In the following discussions, the LBM with the BSBC consists of the combination of Eq. (2.12) with a fixed bridge coefficient: b=0.7, the effective relaxation time by Eq. (2.5) and the D2Q9 discrete velocity model as in [21]. The LBM with the DSBC consists of Eq. (2.13), the effective relaxation time by Eq. (2.6), the regularization procedure Eq. (2.11) and the D2Q21 velocity model as in Niu et al. [12].

During the computations, the criterion

$$\sum_{ij} \left(\frac{|u_{ij}^{(n)} - u_{ij}^{(n-100)}|}{U_b^{(n)}} \right) \leqslant 10^{-6}, \tag{4.1}$$

is applied for the velocity at a lattice node $u_{ij}=u(i,j,t_n)$ to judge the convergence of the solution. Here, the superscript (n) denotes the iteration step and U_b is the bulk mean velocity.

4.1 Force driven Poiseuille flow

The results of the micro flow LBMs by the models with the BSBC and the DSBC are compared in Fig. 3, where H is the channel height. These streamwise velocity U profiles are normalized by the mean velocity U_b. The 2-D uniform Cartesian lattice of 100×100 (this density of the lattice was confirmed to be more than fine enough in [12]) is used for the simulations. The drive force and periodic boundary conditions are applied to the x-direction and thus, the flow
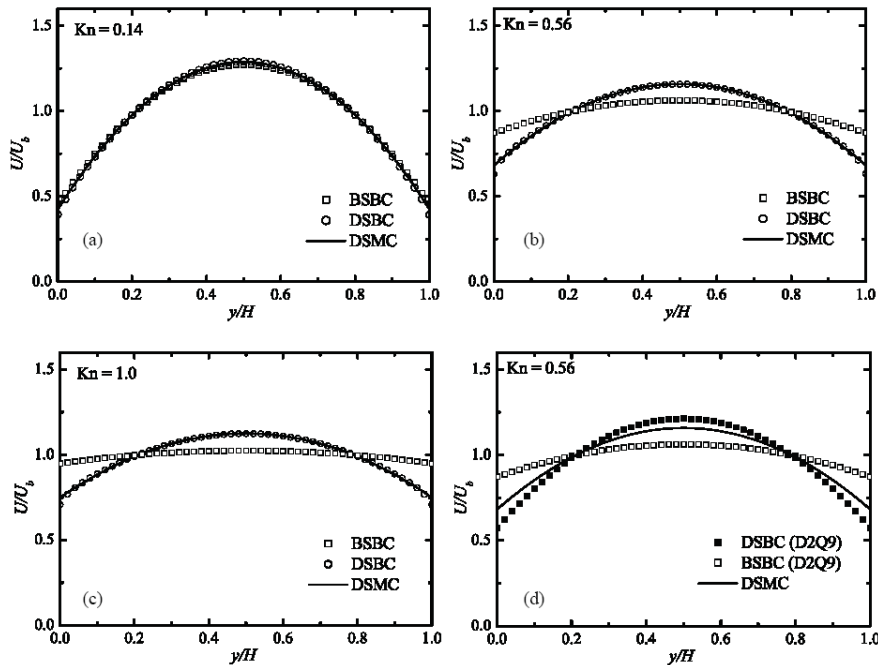

Figure 3: Streamwise velocity profile comparisons by the wall boundary condition models in Poiseuille flows; (a) at Kn=0.14, (b) at Kn=0.56, (c) at Kn=1.0, (d) at Kn=0.56.
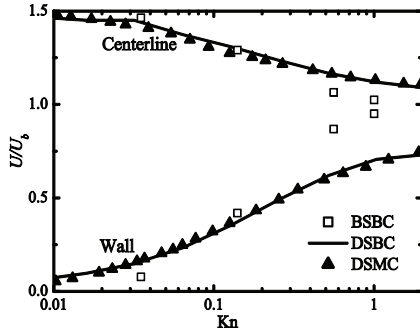
Figure 4: Velocity scaling at wall and centerline of the channels; the DSMC results are from [1].
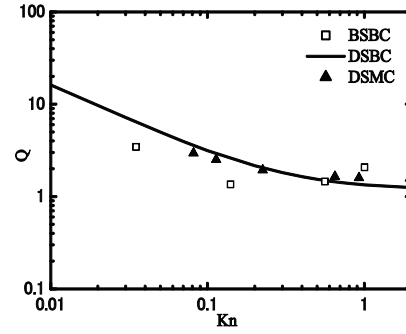

Figure 5: Dependency of the flow rates on Kn; the DSMC results are from [1].

regime is regarded as in a fully developed condition. The number of iterations of the LBM simulations is 5,000 and the results are fully converged. As shown in Fig. 3(a), at Kn=0.14 both models well reproduce the DSMC [1] results with fully diffusive wall boundary conditions (the accommodation coefficient is 1.0). At a little higher Kn cases, Kn≥0.56, the BSBC model overpredicts the slippage though the DSBC works well as shown in Figs. 3(b) and (c). This deterioration in the BSBC is not due to the difference in the discrete models as confirmed in Fig. 3(d). Although the DSBC with the D2Q9 predicts a little worse, it is far better than the BSBC.

The slip and centerline velocities and the mass flow rate

$$Q = \sum_{y=0}^{H} \frac{\rho U(y)}{\left(\rho \mathbf{a}_x H^2 / c_s\right)}, \tag{4.2}$$

are compared in Figs. 4 and 5. It can be seen that the Kn dependency of these values in the BSBC model is also not very reliable compared with that of the DSBC model. Although as shown in Fig. 4 the slip and centerline velocities are reasonably predicted by the BSBC model with b=0.7 at Kn≤0.14, the mass flow rate is somehow underpredicted as in Fig. 5. This implies that the applicability of the presently applied set of model equations with the BSBC model is rather limited. The above observations suggest that in the BSBC, at least the coefficient b should vary depending on Kn even for the fully diffusive walls. Note that in order to satisfy the second order slip boundary condition, Guo et al. [23] showed a functional bridge coefficient (:bounce-back fraction in [23]) which varied as Kn and the lattice spacing. (Their recommended function gives b=0.6, which is close to the currently applied value, for the present computations at Kn=0.14 and 0.56. Indeed, it gives b=0.57 and b=0.63 for Kn=0.14 and 0.56, respectively.) Verhaeghe et al. [13] also proposed a functional bridge coefficient on Kn for the multiple relaxation time LBM.

4.2 Combined nanochannel flow

As shown in Fig. 6, a flow in a nanochannel with an inserted flat plate is considered. For the MD simulation, the mother channel height H and its domain length L are set as respectively 16.5 nm and 32 nm. The inserted flat plate, which makes another narrower channel region, has the thickness of 0.15H and the length of $L/2$. The gap (the height of the finite narrower channel) between the plate and the channel bottom wall is 0.125H. The drive force and periodic boundary conditions are applied to the x-direction and thus, the flow regime
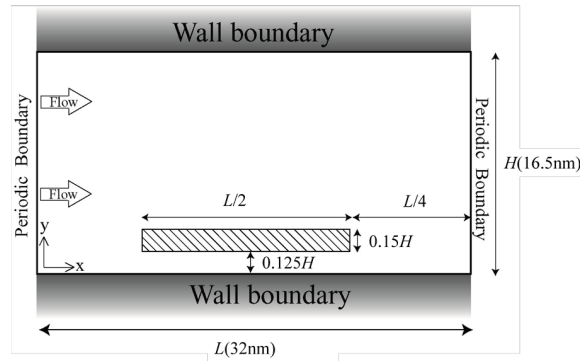
Figure 6: Flow field geometries of the combined nanochannel.

is regarded as a fully developed force-driven nanochannel flow combined with developing narrower nanochannel flows inside. In Table 2, the computational conditions for the MD simulation are summarized. The computational domain shown in Fig. 6 is $92.4\sigma \times 24.9\sigma \times 46.2\sigma$ and 12784 fluid molecules surrounded by 16728 wall molecules of argon mono-layers are simulated. After the process described in the former section, the obtained Knudsen number from the MD simulation is Kn=0.14 based on the characteristic length H. The corresponding LBM simulations are thus carried out on the grid size of 187×97 for the same Kn as that of the MD simulation. After a series of grid dependency tests, results by the grid of 187×97 are guaranteed to be grid independent as shown in Fig. 7, which shows that the result by the 94×49 grid is virtually identical to that by the 187×97 grid. The number of iterations of the LBM simulations is 12,000 and the results are fully converged. Meanwhile, 9 million time steps are required to obtain reasonable flow statistics by the MD simulation.

Table 2: Computational conditions of the MD simulation for a flow in a combined nanochannel.

domain	fluid molecules	wall molecules	Kn
$92.4\sigma \times 24.9\sigma \times 46.2\sigma$	12784	16728	0.14

Fig. 8 compares the normalized streamwise velocity U profiles at x/L=0.0-0.93. Both the
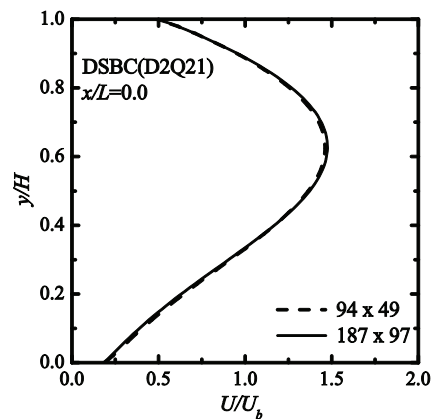

Figure 7: Results of the grid dependency test.

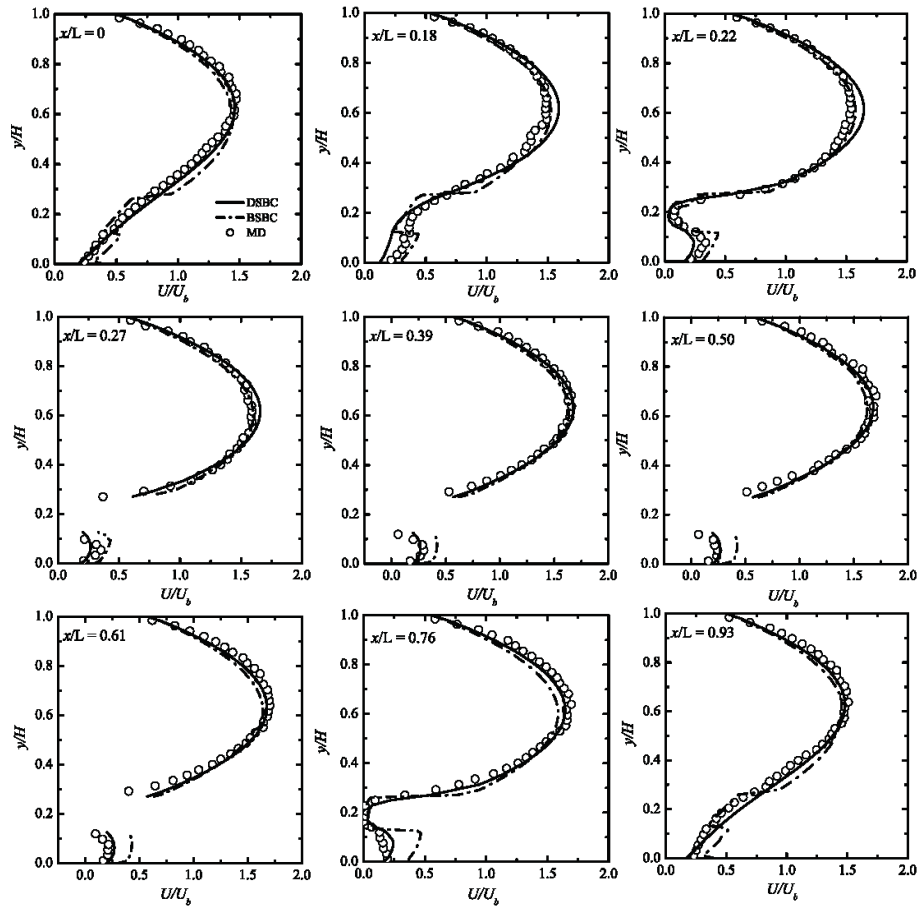Figure 8: Comparison of the development of streamwise velocity profiles in the combined nanochannel flow at Kn=0.14.

results of the LBM simulations by the BSBC and the DSBC models reasonably agree with the general profiles of the MD simulation in the wider gap region since both LBMs satisfactorily predict the Poiseuille flow field at Kn=0.14 (Fig. 3(a)). However, somehow the BSBC model produces unphysical kinks near the edges of the flat plate as in the plots of x/L=0.0, 0.18, 0.93 of Fig. 8. Moreover, the BSBC tends to overpredict the velocity profiles in the narrower channel region of $0.25 < x/L < 0.75$.

This is confirmed in Fig. 9. It is obvious that the flow develops and the profile becomes flatter in the downstream region as indicated by the MD simulation. In fact, the peak velocity tends to be smaller. Although the DSBC model predicts better levels of the velocity profiles, the profiles are somehow almost unchanged. Once the velocity is normalized by the mean velocity inside the narrower channel U_b^*, as shown in Fig. 10, the velocity distribution profiles by the LBMs look similar to the Poiseuille flow at Kn=1.0 of Fig. 3(c) though the profile of the BSBC model shows kinks.

Since the height of the narrower channel region is $0.125H$, the characteristic Knudsen number becomes 1.12 if such a length is chosen. Nonetheless, during the present LBM simulations, the characteristic length is fixed to the mother channel height H. Correspondingly, except for the wall boundary model, the local Kn effect comes from Eq. (2.7) by the variation of the fluid
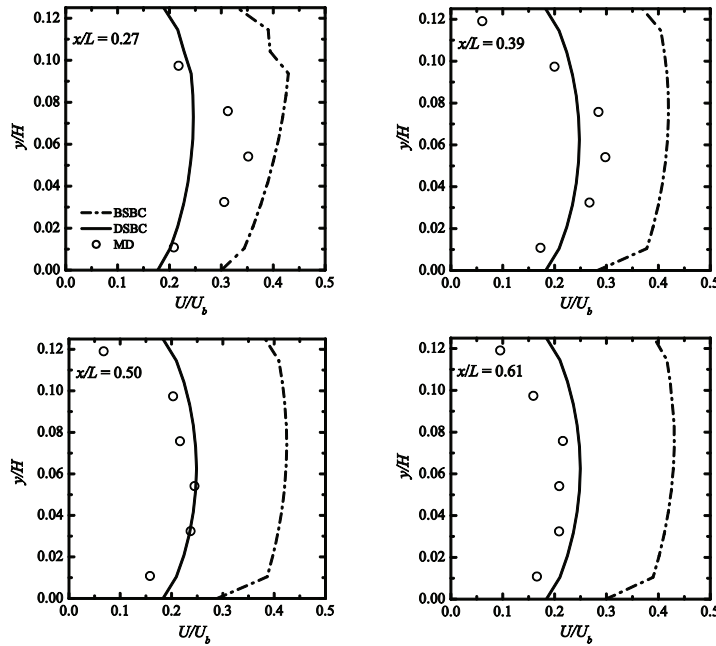
Figure 9: Comparison of the streamwise velocity development in the narrower nanochannel region.

density when the effective relaxation time of Eq. (2.6) is applied. This local effect is, however, not very large in the force driven flows. In the LBM with the BSBC, such a local effect is not included because the effective relaxation time of Eq. (2.5) does not change locally. Therefore, the velocity profiles similar to those of the Poiseuille flow at Kn=1.0 come from the wall boundary models. This means that the relation between the flow rate and the slippage velocity predicted by the wall boundary model controls the velocity profiles. The overprediction of the velocity inside the narrower channel by the BSBC observed in Fig. 8 well corresponds to the overprediction of the flow rate of the Poiseuille flow at Kn=1.0 shown in Fig. 5.

In Fig. 10, the profile by the MD simulation clearly shows that the flow is not fully developed at x/L=0.61 (x/h=4.9, where h=0.125H) since the position is still close to the entrance region. Since it can be considered that this flow development tendency comes from the distribution of the local pressure gradient inside the narrower channel, the effective relaxation time
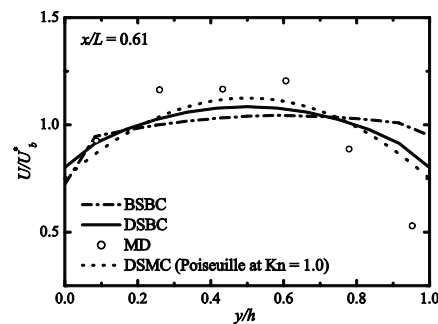

Figure 10: Comparison of the streamwise velocity in the narrow channel; h is the height of the narrow channel region: h=0.125H.
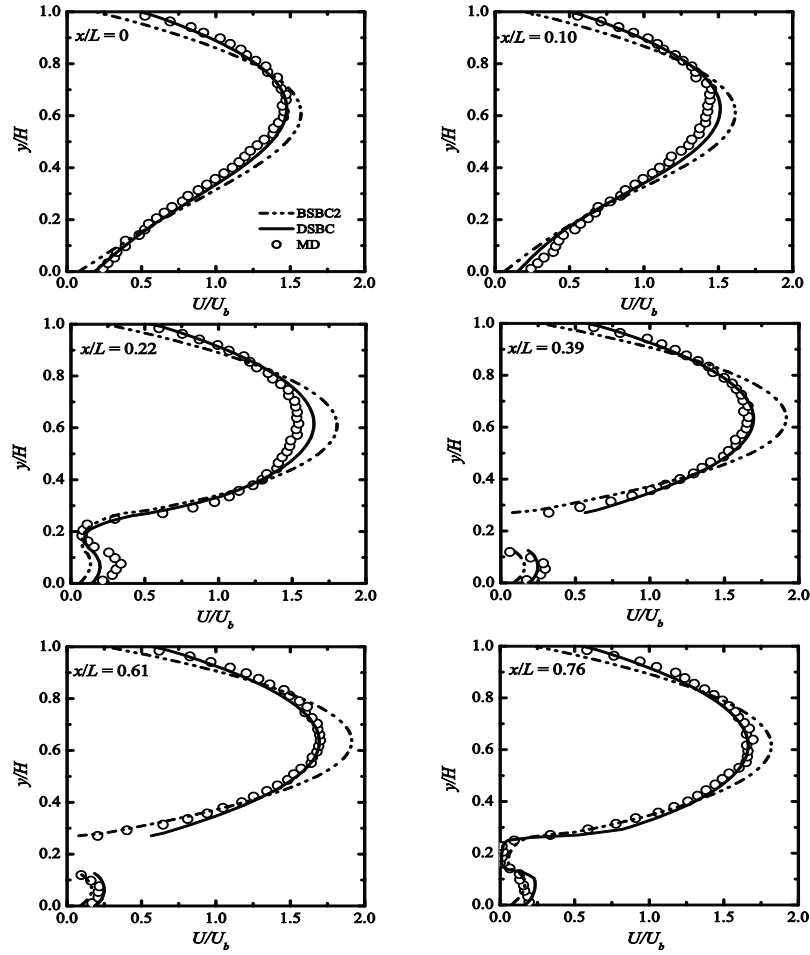
Figure 11: Comparison of the development of streamwise velocity profiles in the combined nanochannel flow at Kn=0.14; BSBC2 denotes BSBC with the regularization by Eq. (2.11) and the relaxation time of Eq. (2.6).

requires to have more sensitivity to the local conditions for capturing this phenomenon.

In order to understand the source of the aforementioned kink profiles of the BSBC model, a further computation by the BSBC with the effective relaxation time of Eq. (2.6) and the regularization process of Eq. (2.11) is performed. Fig. 11 compares this simulation result named BSBC2 with the DSBC result. It is clear that all the kink profiles disappear. Although the distribution profiles become smooth, the agreement with the MD simulation tends to be worse due to the low slippage velocities at the walls. This may be improved by modifying the bridge coefficient b to be smaller than $b=0.7$ in Eq. (2.12).

5   Conclusions

The widely used micro-flow wall-boundary conditions for LBM based on the lattice BGK model are evaluated in a force driven combined nanoscale channel flow at Kn=0.14. To obtain

the reference data, the MD simulation is performed with a fully diffusive wall condition. The LBMs are with the bounce-back/specular reflection and the diffuse scattering wall boundary conditions with additional models for the relaxation time. Although the LBM with the latter boundary model shows generally satisfactory results in the test flow cases including fully developed force driven Poiseuille flows, the former model performs worse at Kn>0.5 in the Poiseuille flows with a fixed bridge coefficient of b=0.7. This causes its overprediction of the flow rate in the narrower channel region since the characteristic Knudsen number there is 1.12. Hence, the bridging coefficient for the bounce-back/specular reflection wall boundary model should have dependency on Kn and local flow quantities. The MD simulation suggests that the flow develops gradually through the narrow channel region whereas both the LBM predictions show almost instant flow development. This result implies that the effective relaxation time model needs to have more sensitivity to the locally defined Knudsen number. Although the widely applied model combination with the bounce-back/specular reflection wall model produces unphysical kinks in the velocity profiles, introducing the regularization process can get rid of the kinks and is necessary for complex nano/micro flow fields.

Acknowledgements

References

[1] G. KARNIADAKIS, A. BESKOK AND N. R. ALURU, Microflows and Nanoflows: Fundamentals and Simulation, Springer, 2005.

[2] C. CERCIGNANI, Theory and Application of the Boltzmann Equation, Scottish Academic Press, Edinburgh, 1975.

[3] S. CHAPMAN AND T. G. COWLING, The Mathematical Theory of Non-Uniform Gases, Cambridge University Press, Cambridge, England, 1970.

[4] X. NIE, G. D. DOOLEN AND S. CHEN, *Lattice-Boltzmann simulations of fluid flows in MEMS*, J. Statist. Phys., 107 (2002), pp.279–289.

[5] S. SUCCI, *Mesoscopic modeling of slip motion at fluid-solid interfaces with heterogeneous catalysis*, Phys. Rev. Lett., 89 (2002), 064502.

[6] S. ANSUMALI AND I. V. KARLIN, *Kinetic boundary conditions in the lattice Boltzmann method*, Phys. Rev. E., 66 (2002), 026311.

[7] Z. GUO AND C. ZHENG, *An extrapolation method for boundary conditions in lattice Boltzmann method*, Phys. Fluids., 14 (2002), pp. 2007–2010.

[8] G. H. TANG, W. Q. TAO AND Y. HE, *Simulation of fluid flow and heat transfer in a plane channel using the lattice Boltzmann method*, Int. J. Modern. Phys. B., 17 (2003), pp. 183–187.

[9] C. SHEN, D. B. TIAN, C. XIE AND J. FAN, *Examination of the LBM in simulation of microchannel flow in transitional regime*, J. Microscale. Thermophysical. Engrg., 8 (2004), pp. 423–432.

[10] F. TOSCHI AND S. SUCCI, *Lattice Boltzmann method at finite Knudsen numbers*, Euro. Phys. Lett., 69 (2005), pp. 549–555.

[11] Y. H. ZHANG, R. QIN AND D. R. EMERSON, *Lattice Boltzmann simulation of rarefied gas flows in microchannels*, Phys. Rev. E., 71 (2005), 047702.

[12] X. D. NIU, T. MUNEKATA, S. HYODO AND K. SUGA, *Kinetic lattice Boltzmann method for microscale gas flows: issues on boundary condition, relaxation time and regularization*, Phys. Rev. E., 76 (2007), 036711.

[13] F. VERHAEGHE, L. S. LUO AND B. BLANPAIN, *Lattice Boltzmann modeling of microchannel flow in slip flow regime*, J. Comput. Phys., 228 (2009), pp. 147–157.

[14] R. ZHANG, X. SHANG, AND H. CHEN, *Efficient kinetic method for fluid simulation beyond the Navier-Stokes equation*, Phys. Rev. E, 74 (2006), 046703.

[15] Z. L. GUO AND C. G. ZHENG, *Lattice Boltzmann methos for micro-scale flows*, Proc. 2nd Asian Symp. Comput. Heat Transf. Fluid Flow, Jeju, Korea, 2009, Paper No. ASCHT09-K11.

[16] G. H. TANG, W. Q. TAO AND Y. HE, *Gas slippage effect on microscale porous flow using the lattice Boltzmann method*, Phys. Rev. E., 72 (2005), 056301.

[17] J. HAILE, Molecular Dynamics Simulation: Elementary Methods, John Wiley & Sons Inc., New York, 1997.

[18] G. R. MCNAMARA AND G. ZANETTI, *Use of the Boltzmann equation to simulate lattice-gas automata*, Phys. Rev. Lett., 61 (1988), pp. 2332–2335.

[19] F. J. HIGUERA AND J. JIMENEZ, *Boltzmann approach to lattice Gas simulations*, Euro. Phys. Lett., 9 (1989), pp. 663–668.

[20] P. L. BHATNAGAR, E. P. GROSS AND M. KROOK, *A model for collision processes in gases, small amplitude processes in charged and neutral one-component systems*, Phys. Rev., 94 (1954), pp. 511–525.

[21] G. H. TANG, W. Q. TAO AND Y. HE, *Lattice Boltzmann method for simulating gas flow in microchannels*, Int. J. Modern. Phys. C., 15 (2004), pp. 335–48.

[22] Z. L. GUO, T. S. ZHAO AND Y. SHI, *Physical symmetry, spatial accuracy, and relaxation time of the lattice Boltzmann equation for micro gas flows*, J. Appl. Phys., 99 (2006), 074903.

[23] Z. L. GUO, B. SHI, T. S. ZHAO AND C. ZHENG, *Discrete effects on boundary conditions for the lattice Boltzmann equation in simulating microscale gas flows*, Phys. Rev. E., 76 (2007), 056704.